# RNA-mediated interaction between the peptide-binding and GTPase domains of the signal recognition particle

Richard J Spanggord[1], Fai Siu[1], Ailong Ke[1] & Jennifer A Doudna[1–4]

The signal recognition particle (SRP) targets nascent proteins to cellular membranes for insertion or secretion by recognizing polypeptides containing an N-terminal signal sequence as they emerge from the ribosome. GTP-dependent binding of SRP to its receptor protein leads to controlled release of the nascent chain into a membrane-spanning translocon pore. Here we show that the association of the SRP with its receptor triggers a marked conformational change in the complex, localizing the SRP RNA and the adjacent signal peptide–binding site at the SRP-receptor heterodimer interface. The orientation of the RNA suggests how peptide binding and GTP hydrolysis can be coupled through direct structural contact during cycles of SRP-directed protein translocation.

The SRP includes a universally conserved GTPase protein responsible for signal peptide recognition and a tightly bound RNA molecule, as well as additional protein components in archaea and eukaryotes[1,2]. In bacteria, signal peptide binding by the SRP—composed of the Ffh protein and 4.5S RNA—directs the translating ribosome to the periplasmic membrane via binding to the translocon-associated receptor GTPase, FtsY. The phylogenetically conserved 4.5S RNA, which is essential *in vivo*[3,4], substantially accelerates the association and dissociation of Ffh and FtsY, as well as the rate of GTP hydrolysis in the complex[5,6]. Although this suggests a direct interaction between the RNA and the GTPase domains of the Ffh-FtsY heterodimer, structural data are not yet available for the intact SRP–FtsY complex.

A crystal structure of the archaeal SRP core revealed that, together, the N-terminal and GTPase domains of Ffh and the C-terminal M domain and its associated SRP RNA form the opposing arms of a U-shaped assembly in which the signal peptide–binding site[7] is ~60 Å away from the GTPase center (**Fig. 1a**)[8]. Crystal structures of the Ffh-FtsY heterodimer showed how bound GTP molecules are shared by both proteins, suggesting a mechanism for the observed mutual GTPase stimulation upon Ffh-FtsY association[9,10]. However, these structures did not provide insights into the function of 4.5S RNA in the SRP–receptor complex because the SRP core structure lacked the FtsY protein, whereas the heterodimer structures lacked the Ffh M domain and the 4.5S RNA. In addition, because the 4.5S RNA–M domain region of the SRP contains the universally conserved signal peptide recognition site[11], these structures cannot explain how peptide binding and GTP hydrolysis are coupled during GTP-dependent cycles of peptide binding and release[12,13]. To understand the structural basis for SRP-receptor interactions, we set out to determine the

conformational arrangement of protein and RNA components in the *Escherichia coli* SRP–receptor complex.

## RESULTS

### Conformational change of SRP upon receptor binding

To determine the location and orientation of the 4.5S RNA in the *E. coli* SRP–FtsY complex, we used site-directed hydroxyl radical probing[14] to identify the relative spatial relationships of specific amino acid positions on Ffh and FtsY with respect to the full-length 4.5S RNA. Using the crystal structures of the archaeal SRP[8] and the *Thermus aquaticus* Ffh–FtsY complex[10] as guides, we began by introducing single cysteine residues at various positions within Ffh that reside within the M domain or along the Ffh-FtsY interface (**Fig. 1a**). Each Ffh protein containing a single cysteine was then coupled with the cysteine-specific hydroxyl radical generator bromo-acetamidobenzyl-EDTA-Fe (BABE-Fe). The BABE-Fe coupling efficiency for each mutant was high, and each conjugated Ffh protein was able to form a saturable complex with the 4.5S RNA and FtsY in the presence of the nonhydrolyzable GTP analog GMPPCP (**Supplementary Figs. 1** and **2** online). Each BABE-Fe–modified Ffh was assembled into an SRP–FtsY complex, and 4.5S RNA cleavage within the complex was analyzed after incubation with peroxide and ascorbate to produce free radicals[15,16].
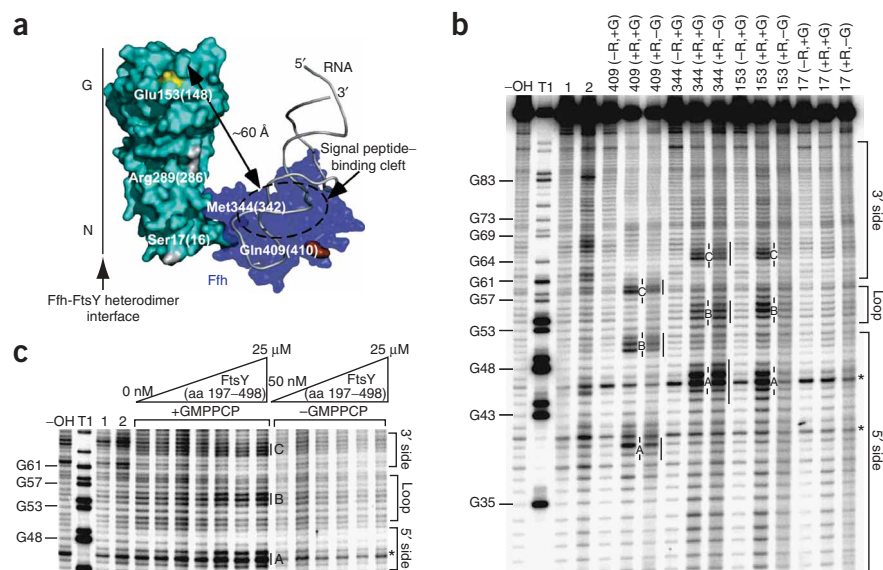
SRP–FtsY complexes containing BABE-Fe–modified sites within the Ffh M domain (residues 344 and 409, **Fig. 1a**) led to 4.5S RNA cleavage at sites close to the RNA tetraloop, consistent with previous crystal structures (**Fig. 1b**, lanes 409 and 344; for quantification of cleavage bands see **Supplementary Fig. 3** online)[8,17]. These cleavage sites occur in the presence or absence of GMPPCP, suggesting that the core structure of the M domain does not change relative to the bound

**Figure 1** Hydroxyl radical probing of the 4.5S RNA by Ffh in the *E. coli* SRP–FtsY (residues 197–498) complex. (**a**) Structure of the archaeal SRP showing the analogous locations of the *E. coli* residues selected for mutagenesis (numbers in parentheses represent the analogous *S. solfataricus* residue numbers)[8]. Residues in contrasting colors represent those BABE-Fe–modified positions that produced localized RNA cleavage sites; residues in white are positions that did not cleave the RNA (see text for details). (**b**) Strand scission of the full-length 4.5S RNA by Ffh in a saturable SRP–FtsY complex derivatized by BABE-Fe at positions 409, 344, 153 and 17 (Ffh positions 53 and 234 are highlighted in **Supplementary Fig. 4**; cleavage from these residues including position 289 is not shown; results are identical to position 17). −OH and T1 indicate 4.5S RNA alkaline hydrolysis and partial T1 RNase cleavage lanes, respectively, and lanes 1 and 2 are 4.5S RNA alone in buffer or in the presence of cleaving reagents, respectively. −G and +G indicate the absence and presence of GMPPCP, respectively.



−R and +R indicate the absence and presence of cleaving reagents, respectively. In **b** and **c**, successive Gs in the RNA sequence are indicated at left, positions of strand scission are indicated by the letters and bars and are further analyzed in **Supplementary Figure 3**, and starred bands represent hyperactive nucleotides that are cleaved in the absence of BABE-Fe–modified Ffh and were not included in the analysis. (**c**) Titration cleavage experiment with Ffh(E153C)–BABE-Fe–labeled SRP with increasing concentrations of FtsY in the presence and absence of GMPPCP. First four gel lanes are as in **b**. Experiments were done with increasing FtsY concentrations as follows: 0 nM, 50 nM, 100 nM, 1 μM, 4 μM, 16 μM and 25 μM. All lanes are in the presence of the cleaving reagents.

4.5S RNA upon GTP-dependent association of Ffh with FtsY. To our surprise, however, SRP–FtsY complexes containing a BABE-Fe–modified site in the Ffh G domain (residue 153) cleaved 4.5S RNA at the same positions as observed with the complex containing BABE-Fe at Ffh residue 344. Furthermore, 4.5S RNA cleavages resulting from the BABE-Fe at residue 153 occurred only in the presence of GMPPCP (**Fig. 1b**, lanes 153; for quantification of cleavage bands see **Supplementary Fig. 3**). These cleavages are saturable as a function of SRP–FtsY complex formation, using either a shorter FtsY construct (residues 197–498) lacking the membrane-association (A) domain[18] or a longer FtsY construct used in a previous study (residues 47–498)[19] (**Fig. 1c** and **Supplementary Fig. 3**, respectively). Because the shorter FtsY construct has similar GTPase activity to that measured for the full-length FtsY[20] and shows more robust complex formation with SRP as assayed by nondenaturing gel mobility shift (**Supplementary Fig. 3**), FtsY (residues 197–498) was used for all further experiments.

The identical sites of 4.5S RNA cleavage produced by BABE-Fe–modified positions 344 and 153 in the SRP–FtsY complex are not consistent with the archaeal SRP crystal structure, in which the sites analogous to the *E. coli* positions 344 and 153 are ∼51 Å apart, well beyond the BABE-Fe probing radius of ∼20 Å (see Methods for our internal calibration of the BABE-Fe probing radius). These cleavage data suggest that in the SRP–FtsY complex, the Ffh M domain and the tetraloop of the 4.5S RNA are near the Ffh G domain, with residues 344 and 153 close together in space. The lack of 4.5S RNA cleavage from BABE-Fe–modified positions 17 and 289 in Ffh (**Fig. 1a,b**, position 17 lanes; position 289, data not shown) supports positioning of the M domain adjacent to the G domain in an orientation that protects the RNA from free radicals produced from these sites. In addition, the observation that BABE-Fe modification at Ffh positions 53 and 234 did not yield any 4.5S RNA cleavage sites implies that the M domain and RNA localize to

one side of the SRP–FtsY complex (**Supplementary Fig. 4** online). Previous cross-linking studies suggested interaction between the Ffh M domain and the FtsY N domain in the absence of 4.5S RNA[21], implying that the linker between the Ffh NG and M domains has the required length to accommodate this conformational rearrangement.

**Orientation of RNA at the SRP-receptor heterodimer interface**

To determine the position and orientation of 4.5S RNA with respect to the Ffh-FtsY heterodimer interface, single cysteine residues were introduced into FtsY along the interface surface (**Fig. 2a**). After BABE-Fe conjugation and testing to confirm full modification and ability to bind SRP as done with the Ffh proteins just discussed, each mutant protein was assembled into an SRP–FtsY complex and 4.5S RNA cleavage was analyzed. Notably, BABE-Fe modification of position 359 in FtsY, located near Ffh position 153 in the heterodimer structure (**Fig. 2a**), results in RNA cleavages near the RNA tetraloop (nucleotides 55–57), where Ffh position 153 also cleaves (nucleotides 54–56) (**Fig. 2b**). As observed with Ffh position 153, BABE-Fe–induced cleavages from FtsY position 359 are saturable and occur only in the presence of GMPPCP, indicating that the RNA is only cleaved upon GTP-dependent formation of the SRP–FtsY complex. Further probing using FtsY containing BABE-Fe at positions 244, 433 or 392 under conditions in which the SRP–FtsY complex is fully formed (**Supplementary Fig. 2**) produced, respectively, 4.5S RNA cleavage sites successively farther away from the tetraloop (**Fig. 2c**; for quantification of the cleavage bands see **Supplementary Fig. 5** online). In contrast, BABE-Fe modification of FtsY at positions 212 and 322 on the back side of the Ffh-FtsY interface (**Supplementary Fig. 4**) produced no specific cleavage patterns in the 4.5S RNA, consistent with the cleavage data from BABE-Fe–modified positions 53 and 234 of Ffh (**Fig. 2c**, position 212 lanes; position 322 data not shown). Mapping the cleavage sites from each BABE-Fe–modified FtsY protein
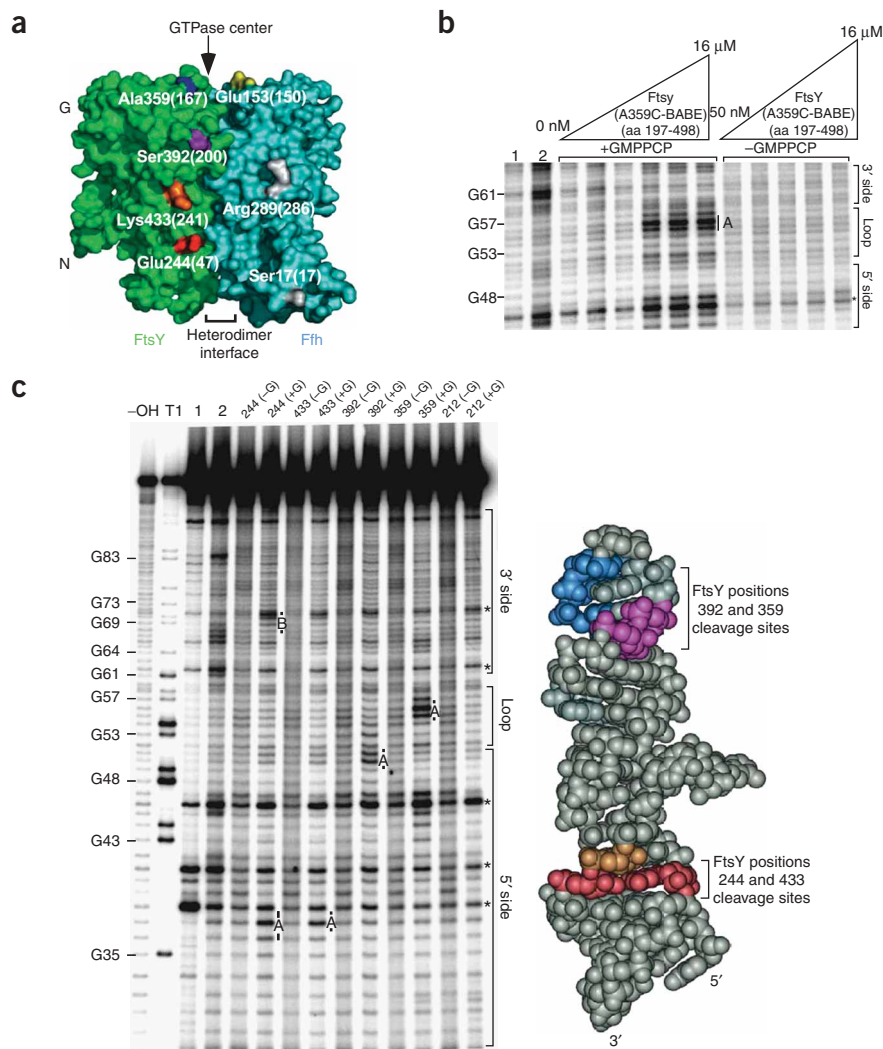
**Figure 2** Hydroxyl radical probing of the 4.5S RNA by FtsY (residues 197–498) in the *E. coli* SRP–FtsY complex. (**a**) Structure of the *T. aquaticus* Ffh and FtsY heterodimer showing the analogous locations of the *E. coli* residues selected for mutagenesis[10] (numbers in parentheses represent the analogous *T. aquaticus* residue numbers). Residues in contrasting colors represent those BABE-Fe positions that produced localized RNA cleavage sites; residues in white are positions that did not cleave the RNA (see text for details). (**b**) Titration cleavage experiment with SRP and increasing concentrations of FtsY(A359C)–BABE-Fe in the presence and absence of GMPPCP. Lanes 1 and 2 are as in **Figure 1** (–OH and T1 are omitted). Experiments were done with increasing FtsY(A359C)–BABE-Fe concentrations as follows: 0 nM, 50 nM, 100 nM, 1 μM, 4 μM and 16 μM. In **b** and **c**, all lanes are in the presence of the cleavage reagents, the cleavage sites are indicated by letters and bars and starred bands represent hyper-reactive nucleotides that are cleaved in the absence of BABE-Fe–modified Ffh and were not included in the analysis. (**c**) Left, strand scission of the full-length 4.5S RNA in a saturated SRP–FtsY complex by FtsY derivatized with BABE-Fe at positions 244, 433, 392, 359 and 212 (**Supplementary Fig. 4**), respectively (for FtsY position 322 (see **Supplementary Fig. 4**), data not shown; result is identical to FtsY position 212). Positions of strand scission are further analyzed in **Supplementary Figure 5**. Right, the tertiary structure of the stem-loop end of the *E. coli* 4.5S RNA (nucleotides 29–76, ref. 17), where the colored nucleotides highlight the FtsY cleavage sites.

onto the 4.5S RNA tertiary structure defines a specific orientation for the bound RNA in which the highly conserved RNA tetraloop is adjacent to the FtsY GTPase domain; the other end of the RNA hairpin abuts the FtsY N domain (**Fig. 2c**, right panel). Notably, all four BABE-Fe–modified FtsY positions and the Ffh 153 position that elicited localized 4.5S RNA cleavage are located on one side (the front) of the Ffh-FtsY heterodimer (**Fig. 2a**). This suggests that the RNA localizes exclusively at or near the front of the Ffh-FtsY heterodimer interface, consistent with the absence of specific RNA cleavage sites produced by BABE-Fe modifications on the back side of the interface (**Supplementary Fig. 4**).

### Model of the SRP–receptor ternary complex
Using distance constraints derived from the BABE-Fe–induced cleavage data and calibrated using available high-resolution crystallographic structures, a molecular model of the *E. coli* SRP–FtsY complex was constructed and refined using torsion-angle molecular dynamics[22] (**Fig. 3a,b**; **Supplementary Fig. 6** online; see Methods). In this model, Ffh and FtsY share the same RNA-binding site, consistent with the observed lack of changes in the footprint of Ffh on the 4.5S RNA upon binding to FtsY[23]. Furthermore, all of the RNA-protein structural contacts occur within the most conserved portion of the 4.5S RNA, consistent with the observation that the

hairpin end of 4.5S RNA is necessary and sufficient for SRP function *in vivo*[17]. The proximity of the Ffh M domain to the N and G domains is also consistent with data from fluorescence and cross-linking studies showing high-affinity interaction between isolated Ffh M and NG domains and domain shifts in Ffh upon binding to the 4.5S RNA and to FtsY[24]. In addition, weak electron density for the linker region between the Ffh M and G domains in a previous crystal structure of the intact *T. aquaticus* Ffh protein suggested linker flexibility[25], and cross-linking showed that even in the absence of the 4.5S RNA, the Ffh M domain can swing into the Ffh-FtsY interface[21].

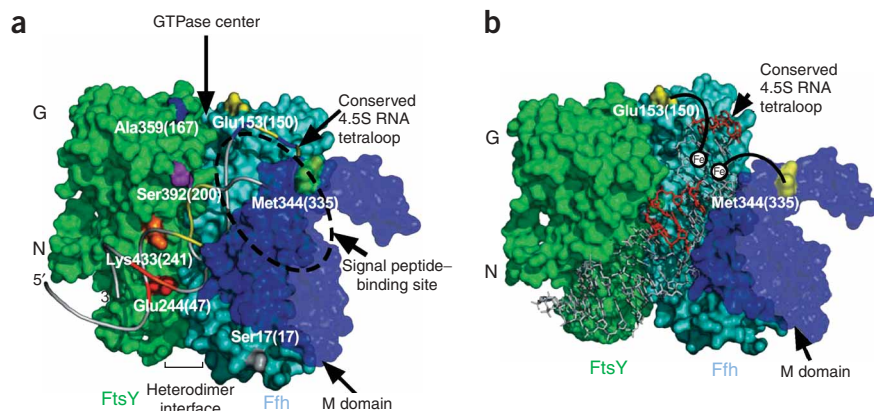### SRP conformational change requires receptor binding
The tethered hydroxyl radical probing data and resulting model show that the 4.5S RNA bridges the Ffh-FtsY interface, but does localization of the RNA to this region occur before or after SRP–FtsY complex formation? One possibility is that both GTP and FtsY are necessary for the observed conformational rearrangement in Ffh. Alternatively, GTP binding to Ffh alone[5] might be sufficient to induce the observed Ffh conformational rearrangement, thus prepositioning the SRP for FtsY binding. To test these possibilities, Ffh containing BABE-Fe–modified position 153 was bound to 4.5S RNA with increasing concentrations of GMPPCP in the presence and absence of FtsY (**Fig. 4a**). Notably, in the absence of FtsY no localized cleavage of the 4.5S RNA with the intensities observed in the previous experiments (**Fig. 1b**) was observed (**Fig. 4a**, –FtsY lanes). However, as before, upon addition of FtsY the

**Figure 3** Molecular model of the *E. coli* SRP–FtsY complex. (**a**) Model of the SRP–FtsY complex was constructed using the hydroxyl radical probing data as spatial constraints to position the 4.5S RNA and M domain in the complex as shown. FtsY and Ffh are depicted in the space-filling mode; FtsY, green; Ffh, blue; M domain, dark blue; signal peptide–binding site, dashed circle; 4.5S RNA, gold. Those BABE-Fe–modified positions that cleaved the 4.5S RNA are highlighted in contrasting colors, and their corresponding cleavage sites are indicated on the RNA in the corresponding colors (numbers in parentheses represent the analogous *T. aquaticus* residue numbers). White residues represent positions that failed to cleave the RNA. (**b**) Location of the two BABE-Fe moieties at Ffh positions 153 and 344, where the cleaved nucleotides are highlighted in red. The cleavage pattern generated from these positions suggests placement of the BABE-Fe in the RNA major groove leading to strand scission in the two adjacent minor grooves (in this case one of the minor grooves is the RNA loop)[36]. The same analysis was done for the FtsY positions in **Supplementary Figure 6**.

previously observed RNA cleavage sites reappeared (**Fig. 4a**, +FtsY lanes; see **Supplementary Fig. 7** online for quantification of cleavage bands). These results show that the association of SRP with its receptor causes the marked conformational rearrangement in the SRP, bringing the 4.5S RNA to the Ffh-FtsY interface and the associated Ffh M domain proximal to the GTPase domains of Ffh and FtsY.

### 4.5S RNA tetraloop affects SRP–receptor GTPase activity

The proximity of the 4.5S RNA tetraloop and the Ffh and FtsY GTPase domains in the SRP–FtsY model raised the possibility that the evolutionarily conserved tetraloop nucleotides directly influence GTPase activity of the SRP–FtsY complex. Hydrolysis of GTP by both Ffh and FtsY is known to be stimulated once the SRP–FtsY complex is formed[26]. In addition, the sequence of the 4.5S RNA tetraloop was previously shown to affect formation of the SRP–FtsY complex[23]. To test for a possible effect of the tetraloop on GTPase activity in the SRP–FtsY complex, a 4.5S RNA mutant was prepared in which the tetraloop was mutated from GGAA to UUCG, a change that causes a lethal phenotype *in vivo* (F. Siu and J.A. Doudna, unpublished data)[23]. Under our reaction conditions, this mutant 4.5S RNA assembles into a stable SRP–FtsY complex as detected by nondenaturing gel mobility shift (**Fig. 4b**), in contrast to results from a previous study[23]. This difference in the behavior of the complex that we observed could arise from an effectively higher concentration of GMPPNP in our experiments, owing to the use of a chromatographically purified GMPPNP sample (see Methods). Notably, the UUCG mutant 4.5S RNA considerably reduced the rate of GTP hydrolysis within the SRP–FtsY complex to nearly the level of Ffh on its own (**Fig. 4c**). These data support the proximity of the 4.5S RNA tetraloop and the GTPase active sites within the SRP–FtsY complex, as proposed in our structural model. Furthermore, the influence of the RNA tetraloop nucleotides on GTP hydrolysis is intriguing because the
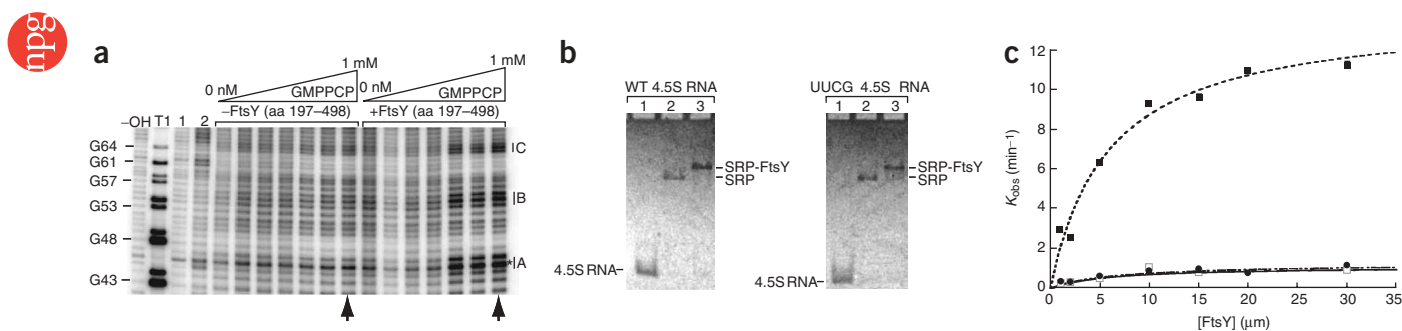


**Figure 4** FtsY (residues 197–498) is required for the observed SRP conformational rearrangement, and the 4.5S RNA tetraloop affects the heterodimer GTPase activity. (**a**) Strand scission of the full-length 4.5S RNA bound by Ffh derivatized by BABE-Fe at position 153 in the absence and presence of FtsY with an increasing amount of GMPPCP (increasing GMPPCP concentrations as follows: 0 nM, 10 nM, 100 nM, 500 nM, 100 μM, 500 μM and 1 mM). Gel labels are as in **Figure 1,** and all protein lanes are in the presence of cleaving reagents. Arrows indicate those lanes used in the quantification analysis (see **Supplementary Fig. 7**). (**b**) Gel mobility shift assay of SRP containing the wild-type (WT) 4.5S RNA and the UUCG tetraloop RNA with FtsY under similar reaction conditions to those reported earlier (see Methods)[23]. WT 4.5S RNA lanes are as follows: lane 1, WT 4.5S RNA alone; lane 2, WT 4.5S RNA + 0.9 nM Ffh; lane 3, WT 4.5S RNA + 0.9 nM Ffh + 1.1 nM FtsY. UUCG 4.5S RNA lanes are the same as the lanes for the WT 4.5S RNA gel except the UUCG tetraloop 4.5S RNA was used. (**c**) GTPase activity of the SRP–FtsY complex. The observed rate of the stimulated GTP hydrolysis by the SRP–FtsY complex was determined with a small fixed amount of Ffh and varying concentrations of FtsY (residues 197–498) in the presence (■) and absence (●) of the 4.5S RNA and in the presence of the UUCG tetraloop 4.5S RNA (□). The maximal rate constants were as follows: $13.8 \pm 0.95$ min$^{-1}$ in the presence of the 4.5S RNA, $1.11 \pm 0.16$ min$^{-1}$ in the absence of the 4.5S RNA and $1.24 \pm 0.13$ min$^{-1}$ in the presence of the UUCG tetraloop 4.5S RNA. $K_{1/2}$ values were as follows: $5.91 \pm 1.26$ μM in the presence of the 4.5S RNA, $5.85 \pm 2.62$ μM in the absence of the 4.5S RNA and $6.17 \pm 2.04$ μM in the presence of the UUCG tetraloop 4.5S RNA.

loop is adjacent to the signal peptide–binding site within the associated M domain of Ffh[7]. Together, these observations imply an RNA-mediated connection between the signal peptide–binding and regulatory centers of the SRP–FtsY complex.

## DISCUSSION

The proposed conformational change in the SRP upon binding to its receptor explains several observations about SRP function that have been puzzling in light of previous structural and biochemical data. First, our model based on the tethered-probe cleavage data depicts an extended RNA interaction surface created by both the Ffh and FtsY proteins, bridging the heterodimer interface. Notably, FtsY alone cannot bind to 4.5S RNA, showing that both Ffh and GMPPCP are necessary to create a stable RNA-recognition site (**Supplementary Fig. 2**)[26]. The RNA conformation induced upon Ffh M domain binding[17] may be a prerequisite to FtsY–4.5S RNA interaction, analogous to SRP19 priming of the 7S RNA to bind the Ffh homolog SRP54 in the mammalian SRP[27,28]. The presence of the 4.5S RNA at the protein-protein interface of the SRP–FtsY complex, where it could influence protein structure or dynamics directly, may explain its 200-fold catalytic effect on SRP-FtsY association and dissociation[6]. Second, the location of the Ffh M domain in the complex would position the bound nascent signal peptide directly adjacent to the GTPase domains of Ffh and FtsY, coordinating productive peptide binding with GTP hydrolysis by the SRP–FtsY complex. The appreciable conformational rearrangement of Ffh and 4.5S RNA orientation discovered in this work is therefore a plausible mechanism for direct communication between the signal peptide–recognition site and GTPase domains of the SRP–FtsY complex. Finally, our results suggest a function for the evolutionarily conserved tetraloop of the 4.5S RNA as a structural and functional link between the signal peptide–binding and regulatory centers of the SRP–receptor complex. The placement and sequence of the 4.5S RNA tetraloop are thus of crucial importance to SRP activity, helping to explain their high level of evolutionary conservation[4].

The Ffh, FtsY and 4.5S RNA interactions clarified here involve SRP components conserved in higher organisms, implying that the conformational rearrangement we describe may also occur in archaeal and eukaryotic SRPs. In support of this possibility, previous cross-linking studies with the ribosome-bound mammalian SRP showed conformational rearrangements in SRP54 upon receptor binding to the complex[29]. This suggests that the observed conformational rearrangement in the *E. coli* SRP could take place on the ribosome. Comparison of our structural model to that of the mammalian SRP bound to the 80S ribosome[30], determined by single-particle cryo-EM, reveals some similarities. In the cryo-EM structure, modeling of SRP54 on the ribosome with a bound signal peptide suggested that the G domain of SRP54 is oriented in between the N and M domains and adjacent to the M domain–associated SRP RNA[30,31]. From this analysis it was predicted that the signal peptide–binding site may be positioned near the GTPase domain of SRP54, similar to our model of the *E. coli* SRP–FtsY complex[32]. Differences in the placement of the conserved tetraloop relative to the SRP54–Ffh G domain in the two models may be due to the absence of the mammalian SRP receptor in the cryo-EM structure and to the presence of additional RNA and protein components in the mammalian SRP. The conformational rearrangement we detect in the SRP receptor may occur on the ribosome upon receptor binding or could be a structural change relevant to the postribosome SRP–FtsY complex. It is tempting to propose that the observed conformational change in the *E. coli* SRP upon receptor binding acts as a molecular switch to signal the ribosome that the SRP receptor is bound. Indeed, this conformational switch could also influence the affinity of the SRP–FtsY complex for the ribosomal exit site, thus providing a mechanistic precursor to shuttling the ribosome to the translocon upon productive signal peptide and receptor binding.

## METHODS

**Protein and RNA expression and purification.** Cloning of the wild-type and UUCG tetraloop 4.5S RNAs was done as described in ref. 33. In these studies we used two different N-terminally truncated versions of FtsY (one construct consists of residues 197–498 and the other construct consists of residues 47–498) and a C-terminally truncated version of Ffh (residues 1–432), which respectively form the heterodimer complex and bind RNA with wild-type affinities (data not shown). Cloning of Ffh and FtsY (residues 197–498) containing an N-terminal $His_6$ tag was done as described in ref. 33. A protein-expression plasmid encoding FtsY (residues 47–498) was generously provided by Shu-ou Shan (California Institute of Technology, Pasadena, California, USA). Site-directed mutagenesis of Ffh and FtsY (residues 197–498) was carried out with the QuikChange site-directed mutagenesis kit (Stratagene). The only endogenous cysteine in the SRP–FtsY complex, at position 406 of Ffh, was mutated to a serine to produce a cysteine-free Ffh protein[33]. Incorporation of single cysteines into Ffh and FtsY was verified by sequencing of all constructs.

FtsY (residues 47–498) was expressed and purified as described in ref. 5. The native and single-cysteine Ffh and FtsY (residues 197–498) proteins were expressed and purified as follows. The Ffh and FtsY expression vectors were transformed into *E. coli* BL21 (DE3) cells expressing pLysS. Freshly transformed cells were grown in 750 ml LB medium supplemented with 100 μg ml$^{-1}$ ampicillin and 34 μg ml$^{-1}$ chloramphenicol at 37 °C until the absorbance at 600 nm reached 0.4. Protein expression was induced with 0.5 mM IPTG, and the cells were grown at 28 °C for an additional 3.5 h. Cells were harvested by centrifugation (7,000 r.p.m. in a Beckman JA-10 rotor) and resuspended in cell lysis buffer (50 mM Tris (pH 7.5), 300 mM NaCl, 10 mM $MgCl_2$, 10% (v/v) glycerol, 5 mM β-mercaptoethanol (β-ME), 1% Triton X-100 (v/v)). Lysozyme (40 μg ml$^{-1}$ final concentration) was added to the cell resuspension, which was then frozen at –80 °C. Cell resuspensions were thawed at 37 °C for 10 min, and 20 mM $MgSO_4$, 2 mM $CaCl_2$, 100 units of RNase-free DNase, 50 μg ml$^{-1}$ PMSF and 10 μg ml$^{-1}$ leupeptin were added and incubated for 30 min at 4 °C, then for 20 min at 37 °C. Cell resuspensions were centrifuged at 10,000*g* for 1 h, and the cell lysates were removed.

Crude cell lysates were applied to a 5-ml bed volume containing Superflow $Ni^{2+}$ resin (Qiagen) equilibrated with the following buffer: 50 mM Tris (pH 7.5), 300 mM NaCl, 10% (v/v) glycerol, 5 mM β-ME, 5 mM imidazole). The nickel–nitrilotriacetic acid slurry was washed with five column volumes of the buffer just described and five column volumes of the same buffer supplemented with 10 mM imidazole. The proteins were eluted by adding five column volumes of the same buffer supplemented with 400 mM imidazole and analyzed by SDS-PAGE.

To remove the histidine tag, 1 mg of recombinant $His_6$-tagged tobacco etch virus (TEV) protease was added to the nickel-purified proteins and incubated at 4 °C for 48 h in TEV cleavage buffer (50 mM Tris, pH 7.5, 300 mM NaCl, 10% (v/v) glycerol, 5 mM β-ME). The TEV reactions were applied to a 5-ml bed volume containing Superflow $Ni^{2+}$ resin (Qiagen) equilibrated with buffer (50 mM Tris (pH 7.5), 300 mM NaCl, 10% (v/v) glycerol, 5 mM β-ME, 5 mM imidazole) to remove the cleaved histidine tag and TEV protease. Cleaved Ffh samples were applied to a Mono-S column (Pharmacia) equilibrated in buffer A (50 mM Tris (pH 8.0), 10% (v/v) glycerol, 5 mM DTT, 0.5 mM EDTA). Ffh was eluted using a 17–column volume linear gradient to 100% buffer B (50 mM Tris (pH 8.0), 1 M NaCl, 10% (v/v) glycerol, 5 mM DTT, 0.5 mM EDTA). Cleaved FtsY samples were dialyzed into the following buffer overnight at 4 °C: 50 mM MES (pH 6.0), 100 mM NaCl, 10 mM $MgCl_2$, 10% (v/v) glycerol. They were then applied to a Mono-S column equilibrated in buffer C (50 mM MES (pH 6.0), 10 mM $MgCl_2$, 10% (v/v) glycerol) and eluted using a 16–column volume linear gradient to 100% buffer D (50 mM MES (pH 6.0), 1 M NaCl, 10 mM $MgCl_2$, 10% (v/v) glycerol). Mono-S fractions were analyzed by SDS-PAGE, combined and concentrated to a final concentration of 50–100 μM. Protein concentrations were estimated by Bio-Rad protein assays. All

purified proteins were dialyzed overnight at 4 °C into storage buffer (50 mM Tris (pH 7.5), 300 mM NaCl, 20% (v/v) glycerol, 1 mM DTT) and stored at –80 °C.

**BABE-Fe modification of single-cysteine proteins.** Conjugation of the single-cysteine Ffh and FtsY proteins with the nucleic acid–cleaving reagent BABE-Fe was done initially by incubating 1 ml of a 50–100 µM protein solution with 1 mM DTT for 5 min at room temperature before a 3-h dialysis into degassed modification buffer (50 mM Tris (pH 8.0), 300 mM NaCl, 10% (v/v) glycerol) until all of the DTT had been removed. Each 1 ml of protein solution was divided into two 500-µl samples, of which one was mixed with 2 µl of a 250 mM BABE-Fe solution (in DMSO) and the other was mixed with 2 µl DMSO. Each protein sample was incubated at room temperature for 6 h in the dark. Once the conjugation reaction was complete, 49 µl of each reaction was removed and reacted with 1 µl of 1.5 mM fluorescein and incubated at room temperature for 20 min in the dark. Each fluorescein reaction was filtered to remove any unreacted fluorescein using Micro Bio-Spin 6 columns (Bio-Rad), and 10 µl of these reactions were applied to a 10% SDS-PAGE gel. The extent of BABE-Fe conjugation was analyzed on a 310-nm UV table (**Supplementary Fig. 1**) and by electrospray ionization mass spectrometry. The residual BABE-Fe conjugation reactions were quenched by removing any excess BABE-Fe by dialysis overnight into storage buffer (50 mM HEPES (pH 7.5), 150 mM potassium acetate, 1.5 mM magnesium acetate). BABE-Fe–modified proteins were stored at –20 °C.

**SRP–FtsY complex formation.** The complex between BABE-Fe–modified Ffh, FtsY and 4.5S RNA was observed using gel mobility shift assays (**Supplementary Fig. 2**). 4.5S RNA (300 nM) was incubated with Ffh–BABE-Fe or native Ffh (1 µM) in a buffer containing 50 mM HEPES (pH 7.5), 150 mM potassium acetate, 1.5 mM magnesium acetate and 1 mM GMPPCP for 5 min at room temperature to form the SRP. RNA was heated to 90 °C for 1 min and cooled on ice for 1 min before use. FtsY–BABE-Fe or native FtsY (4 µM) was incubated with the SRP at room temperature in the dark for 30 min (30 µl final reaction volume). After the incubation, 10 µl of an 80% (v/v) glycerol solution was added to the binding reactions and loaded onto a 6% nondenaturing gel. Complexes were visualized by SYBR Gold staining (Molecular Probes) on a 310-nm UV table. For the gel mobility shift assay of SRP containing the wild-type 4.5S RNA and the UUCG tetraloop RNA (**Fig. 4b**), 1 nM wild-type or UUCG tetraloop 4.5S RNA in the presence of GMPPNP (200 µM, Mono-Q purified) was used with 0.9 nM Ffh and 1.1 nM FtsY (residues 197–498) in a 20-µl final reaction volume. Gel mobility shift assays of this kind were also conducted under the kinetic assay conditions, and SRP–FtsY complexes were observed with both RNAs (data not shown).

**Affinity cleaving assays.** SRP–FtsY complexes were preformed as described earlier except that the binding reactions were spiked with $\gamma$-$^{32}$P 5′ end–labeled 4.5S RNA. After incubation as described earlier, cleavage of the RNA was initiated by the addition of hydrogen peroxide and sodium ascorbate (final concentration of 0.01% (v/v) and 5 mM, respectively) followed by a 2-min incubation at room temperature. Distilled water was added to each sample, and two successive phenol extractions and ethanol precipitation of the RNA were then performed. Cleaved 4.5S RNA was resuspended in formamide loading dye and analyzed on a 12% denaturing gel. Data were obtained from the gels using storage phosphor autoradiography and a STORM PhosphorImager (Molecular Dynamics).

**Quantification of cleavage bands.** BABE-Fe cleavage sites were analyzed and quantified using procedures described before[34]. Briefly, individual band intensities were quantitated by PhosphorImager analysis, wherein traces were drawn down the cleavage lanes and their corresponding background lanes (see **Supplementary Figs. 3**, **5** and **7**).

**SRP–FtsY complex model building and refinement.** SWISS-MODEL (http://swissmodel.expasy.org//SWISS-MODEL.html) was used to generate the structural model of the *E. coli* Ffh-FtsY heterodimer using the *T. aquaticus* structure as a template (PDB entry: 1RJ9)[10]. The model, which contains residues 14–295 of Ffh and 224–495 of FtsY, was further refined using torsion-angle molecular dynamics with CNS[22] to remove minor steric clashes.

Inspection of the *E. coli* M domain bound to the 4.5S RNA structure (PDB entry: 1DUL)[17] reveals that the probing distances between the Cα atom of the BABE-Fe–labeled Gln409 and the 2′-hydroxyl of the cleaved RNA bases are in the range of 17.5 ± 7.5 Å. This observation was used as a molecular ruler to calibrate the rest of the distance constraints between the 4.5S RNA and BABE-Fe–modified residues on Ffh and FtsY proteins. An NOE signal was assigned between the Cα atom of the labeled residue and the 2′-hydroxyl of the RNA base for each of the cleavage signals with the average distance, $d_{minus}$ and $d_{plus}$ values set to 17.5 Å, 7.5 Å and 7.5 Å, respectively, using the $r^{-6}$ averaging option.

The initial structural model was generated using restrained rigid body refinement[35]. The NG domain heterodimer and the M domain–RNA complex were treated as two rigid bodies, whose position and orientation were systematically varied until all NOE constraints were satisfied. The model was further refined by introducing additional NOE constraints between residues 393 and 400 of the M domain and residues 17 and 289 of the Ffh NG domain. The resulting structural model was refined using restrained torsion-angle molecular dynamics to resolve minor steric clashes between various parts of the model. The Ffh-FtsY heterodimer and M domain–RNA complexes were refined in different starting orientations and spatial arrangements, which produced similar structural models after refinement.

The M domain finger loop from the *T. aquaticus* crystal structure (PDB entry: 2FFH)[25] was used to model the missing counterpart in the *E. coli* crystal structure (Leu338–Asp370). Similarly, residues Gly293–Glu318 in the *Sulfolobus solfataricus* SRP crystal structure (PDB entry: 1QZW)[8] were used to model part of the missing linker (Gly296–Ser321) connecting the M domain and the NG domains of the *E. coli* Ffh. The two structures were aligned, and the linker in the *S. solfataricus* structure was then moved to pack against the M domain in the model using a simple swinging motion. An additional 7-residue linker was engineered to model the rest of the linker (Lys322–Gly338) lacking in the *E. coli* model.

**GTPase activity assays.** The GTPase activity of the SRP–FtsY complex was measured in several turnover reactions as described in ref. 5. Briefly, all GTPase reactions were carried out at 25 °C in the following buffer: 50 mM HEPES (pH 7.5), 150 mM potassium acetate, 1.5 mM magnesium acetate, 0.01% (v/v) Nikkol and 2 mM DTT. The observed rate of the stimulated GTP hydrolysis by the SRP–FtsY complex was determined with a small fixed amount of Ffh and varying concentrations of FtsY (residues 197–498) in the presence and absence of the 4.5S RNA (1 µM and 5 µM Ffh with and without RNA present, respectively) and in the presence of the UUCG tetraloop 4.5S RNA (5 µM Ffh). A two-fold excess of RNA relative to Ffh was used in this analysis (2 µM wild-type 4.5S RNA and 10 µM UUCG tetraloop 4.5S RNA). FtsY (residues 197–498) concentrations used were as follows: 1, 2, 5, 10, 20 and 30 µM. The reactions were initiated by adding a 100-µM final concentration of fast protein liquid chromatography–purified GTP doped with gel-purified [$\gamma$-$^{32}$P]GTP, and each reaction was monitored and kinetic rates were estimated as described in ref. 5.

*Note: Supplementary information is available on the Nature Structural & Molecular Biology website.*

COMPETING INTERESTS STATEMENT
The authors declare that they have no competing financial interests.

1. Keenan, R.J., Freymann, D.M., Stroud, R.M. & Walter, P. The signal recognition particle. *Annu. Rev. Biochem.* **70**, 755–775 (2001).
2. Doudna, J.A. & Batey, R.T. Structural insights into the signal recognition particle. *Annu. Rev. Biochem.* **73**, 539–557 (2004).
3. Brown, S. & Fournier, M.J. The 4.5S RNA gene of *Escherichia coli* is essential for cell growth. *J. Mol. Biol.* **178**, 533–550 (1984).

4. Larsen, N. & Zwieb, C. SRP-RNA sequence alignment and secondary structure. *Nucleic Acids Res.* **19**, 209–215 (1991).
5. Peluso, P., Shan, S.-O., Nock, S., Herschlag, D. & Walter, P. Role of SRP RNA in the GTPase cycles of Ffh and FtsY. *Biochemistry* **40**, 15224–15233 (2001).
6. Peluso, P. *et al.* Role of 4.5S RNA in assembly of the bacterial signal recognition particle with its receptor. *Science* **288**, 1640–1643 (2000).
7. Zopf, D., Bernstein, H.D., Johnson, A.E. & Walter, P. The methionine-rich domain of the 54 kd protein subunit of the signal recognition particle contains an RNA binding site and can be crosslinked to a signal sequence. *EMBO J.* **9**, 4511–4517 (1990).
8. Rosendal, K.R., Wild, K., Montoya, G. & Sinning, I. Crystal structure of the complete core of archaeal signal recognition particle and implications for interdomain communication. *Proc. Natl. Acad. Sci. USA* **100**, 14701–14706 (2003).
9. Focia, P.J., Shepotinovskaya, I.V., Seilder, J.A. & Freymann, D.M. Heterodimeric GTPase core of the SRP targeting complex. *Science* **303**, 373–377 (2004).
10. Egea, P.F. *et al.* Substrate twinning activates the signal recognition particle and its receptor. *Nature* **427**, 215–221 (2004).
11. Bernstein, H.D., Zopf, D., Freymann, D.M. & Walter, P. Functional substitution of the signal recognition particle 54-kDa subunit by its *Escherichia coli* homolog. *Proc. Natl. Acad. Sci. USA* **90**, 5229–5233 (1993).
12. Song, W., Raden, D., Mandon, E.C. & Gilmore, R. Role of Sec61 in the regulated transfer of the ribosome-nascent chain complex from the signal recognition particle to the translocation channel. *Cell* **100**, 333–343 (2000).
13. Shan, S.-O. & Walter, P. Co-translational protein targeting by the signal recognition particle. *FEBS Lett.* **579**, 921–926 (2005).
14. Culver, G.M. & Noller, H.F. Directed hydroxyl radical probing of RNA from iron(II) tethered to proteins in ribonucleoprotein complexes. *Methods Enzymol.* **318**, 461–475 (2000).
15. Hertzberg, R.P. & Dervan, P.B. Cleavage of DNA with methidiumpropyl-EDTA-iron(II): reaction conditions and product analyses. *Biochemistry* **23**, 3934–3945 (1984).
16. Joseph, S., Weiser, B. & Noller, H.F. Mapping the inside of the ribosome with an RNA helical ruler. *Science* **278**, 1093–1098 (1997).
17. Batey, R.T., Rambo, R.P., Lucast, L., Rha, B. & Doudna, J.A. Crystal structure of the ribonucleoprotein core of the signal recognition particle. *Science* **287**, 1232–1239 (2000).
18. Eitan, A. & Bibi, E. The core *Escherichia coli* signal recognition particle receptor contains only the N and G domains of FtsY. *J. Bacteriol.* **186**, 2492–2494 (2004).
19. Powers, T. & Walter, P. Co-translational protein targeting catalyzed by the *Escherichia coli* signal recognition particle and its receptor. *EMBO J.* **16**, 4880–4886 (1997).
20. Shan, S.-O. & Walter, P. Induced nucleotide specificity in a GTPase. *Proc. Natl. Acad. Sci. USA* **100**, 4480–4485 (2003).
21. Chu, F. *et al.* Unraveling the interface of signal recognition particle and its receptor by using chemical cross-linking and tandem mass spectrometry. *Proc. Natl. Acad. Sci. USA* **101**, 16454–16459 (2004).
22. Brunger, A.T. *et al.* Crystallography & NMR system: a new software suite for macromolecular structure determination. *Acta Crystallogr. D* **54**, 905–921 (1998).
23. Jagath, J.R. *et al.* Important role of the tetraloop region of 4.5S RNA in SRP binding to its receptor FtsY. *RNA* **7**, 293–301 (2001).
24. Buskiewicz, I., Kubarenko, A., Peske, F., Rodnina, M.V. & Wintermeyer, W. Domain rearrangement of SRP protein Ffh upon binding 4.5S RNA and the SRP receptor FtsY. *RNA* **11**, 947–957 (2005).
25. Keenan, R.J., Freymann, D.M., Walter, P. & Stroud, R.M. Crystal structure of the signal sequence binding subunit of the signal recognition particle. *Cell* **94**, 181–191 (1998).
26. Miller, J.D., Bernstein, H.D. & Walter, P. Interaction of *E. coli* Ffh/4.5S ribonucleoprotein and FtsY mimics that of mammalian signal recognition particle and its receptor. *Nature* **367**, 657–659 (1994).
27. Diener, J.L. & Wilson, C. Role of SRP19 in assembly of the *Archaeoglobus fulgidus* signal recognition particle. *Biochemistry* **39**, 12862–12874 (2000).
28. Hainzl, T., Huang, S. & Sauer-Eriksson, A.E. Structural insights into SRP RNA: an induced fit mechanism for SRP assembly. *RNA* **11**, 1043–1050 (2005).
29. Pool, M.R., Stumm, J., Fulga, T.A., Sinning, I. & Dobberstein, B. Distinct modes of signal recognition particle interaction with the ribosome. *Science* **297**, 1345–1348 (2002).
30. Halic, M. *et al.* Structure of the signal recognition particle interacting with the elongation-arrested ribosome. *Nature* **427**, 808–814 (2004).
31. Wild, K., Halic, M., Sinning, I. & Beckmann, R. SRP meets the ribosome. *Nat. Struct. Mol. Biol.* **11**, 1049–1053 (2004).
32. Halic, M. & Beckmann, R. The signal recognition particle and its interactions during protein targeting. *Curr. Opin. Struct. Biol.* **15**, 116–125 (2005).
33. Batey, R.T., Sagar, M.B. & Doudna, J.A. Structural and energetic analysis of RNA recognition by a universally conserved protein from the signal recognition particle. *J. Mol. Biol.* **307**, 229–246 (2001).
34. Strobel, S.A. & Shetty, K. Defining the chemical groups essential for *Tetrahymena* group I intron function by nucleotide analog interference mapping. *Proc. Natl. Acad. Sci. USA* **94**, 2903–2908 (1997).
35. Ubbink, M., Ejdeback, M., Karlsson, B.G. & Bendall, D.S. The structure of the complex of plastocyanin and cytochrome *F*, determined by paramagnetic NMR and restrained rigid-body molecular dynamics. *Structure* **6**, 323–335 (1998).
36. Oakley, M.G. & Dervan, P.B. Structural motif of the GCN4 DNA binding domain characterized by affinity cleaving. *Science* **248**, 847–850 (1990).